STOMATOPOD ANTENNULE DESIGN: THE ASYMMETRY, SAMPLING EFFICIENCY AND ONTOGENY OF OLFACTORY FLICKING

K. S. MEAD* AND M. A. R. KOEHL

Department of Integrative Biology, VLSB 3060, University of California at Berkeley, Berkeley, CA 94720-3140, USA

*e-mail: kmead@socrates.berkeley.edu

Summary

Many crustaceans detect odors from distant sources using chemosensory sensilla (aesthetascs) on their antennules. The greater the flow of water through arrays of aesthetascs, the faster the access of odorant to receptors inside the aesthetascs. Stomatopods facilitate odorant access by flicking their antennules, thus increasing the relative velocity of the water reaching their aesthetascs. We used dynamically scaled physical models to investigate how aesthetasc size and spacing and antennule flicking velocity affect flow penetration into the simple aesthetasc arrays of the stomatopod *Gonodactylaceus mutatus*. Particle image velocimetry of flow fields near models of juvenile and adult antennules revealed that velocity gradients around the aesthetascs are steeper during the outward part of the flick than during the return stroke and that the velocity gradients are steeper at the aesthetasc tips than at their bases. More fluid per unit time flows between aesthetasc rows during the outward stroke than during the return stroke, ensuring that odor sampling is pulsatile. During flicking, velocity gradients are steeper near adult aesthetascs than near juvenile aesthetascs, and adults process more fluid per unit time than juveniles. The resulting differences in odorant access can be related to size- and age-dependent changes in stomatopod ecology.

Key words: stomatopod, mantis shrimp, *Gonodactylaceus mutatus*, aesthetasc, antennule flicking, chemosensory, biomechanics, velocity gradient, particle image velocimetry, olfaction.

Introduction

Chemoreception in the marine environment

Many marine crustaceans rely heavily on olfaction to find food, mates and a suitable habitat and to avoid predators (Ache, 1982; Atema and Voigt, 1995; Zimmer-Faust, 1989). Crustaceans gather chemical information from distant odor sources by means of specialized chemosensory sensilla called aesthetascs located on the antennules (Heimann, 1984; Hallberg et al., 1993). Successful chemoreception requires that the odorant molecules that make up the chemical signal be transported to the aesthetasc surface. Previous studies examining fluid flow around rows of cylinders suggested that the size and spacing of the cylinders affects fluid penetration (Cheer and Koehl, 1987; Hansen and Tiselius, 1992; Koehl, 1993, 1995, 1996a). We hypothesize, therefore, that the morphology of the aesthetascs, their arrangement on the antennules and the movement of the antennules relative to the ambient water motion will affect the flow of fluid containing odorant molecules around the sensilla. This, in turn, will affect the transport of odorants to the aesthetasc surface and thus to the chemoreceptors within the sensilla.

Stomatopods are good model systems for studies of flow and olfaction

We use stomatopod antennules here as a model system for examining the effects of aesthetasc size and spacing and antennule motion on odorant access in marine crustaceans. Stomatopods are aggressive, shrimp-like crustaceans that form burrows in mudflats and coral rubble in semi-tropical and tropical regions and are excellent subjects for chemosensory studies for several reasons. They depend on chemosensory information for several critical aspects of their life history, including feeding, reproduction, investigating burrows and mediating aggressive interactions with conspecifics (Caldwell, 1979, 1985, 1987; Caldwell et al., 1989). The simple arrangement of aesthetascs on their antennules (Mead et al., 1999) facilitates physical and mathematical modeling and contrasts with the complex aesthetasc morphologies seen in crabs and lobsters (Derby, 1982; Derby et al., 1997; Gleeson, 1982; Gleeson et al., 1993; Grünert and Ache, 1988; Hallberg et al., 1992). Post-metamorphic animals are available in a large range of sizes so that we can examine how antennule design and function change with size. In this study, we concentrate on the subtidal tropical Hawaiian stomatopod *Gonodactylaceus mutatus*.

Flicking, fluid flow and olfaction

Many crustaceans sample their chemical environment by rapidly moving their antennules through the surrounding fluid in what is generally termed an antennular flick (Snow, 1973; Schmitt and Ache, 1979; Devine and Atema, 1982; Gleeson et

al., 1993, 1996; Hallberg et al., 1997). Since stomatopods flick their antennules not just to sample odors but also (albeit quite differently) as part of their social display (Caldwell, 1979, 1992), we use the phrase olfactory flick to indicate an antennule flick with an olfactory function.

When stomatopods move their antennules in an olfactory flick, the layer of fluid in contact with the antennular surface does not slip relative to the surface. This results in the development of a velocity gradient (boundary layer) in the fluid between the moving antennular surface and the stationary fluid around it (e.g. Vogel, 1994). The thickness of the boundary layer can affect odorant capture because the rate at which odorant molecules can cross the boundary layer to get to the aesthetasc surface (and to the chemoreceptors within the aesthetasc) depends on the slow process of molecular diffusion. Thick boundary layers slow down odorant access, while thin boundary layers permit relatively rapid access to the aesthetasc surface.

Boundary layers, physical models and Reynolds number

We chose to analyze the boundary layer surrounding aesthetascs in *G. mutatus* during olfactory flicking by visualizing flow around dynamically scaled physical models. This approach facilitates the study of boundary layers around small objects, since it is easy to quantify small-scale flow fields around large models moving slowly, and also enables combinations of variables not found in nature (see Koehl, 1995) to be analysed. To ensure that the ratios of velocities around the model and the real antennule are the same at analogous positions in the flow field, the Reynolds numbers describing fluid flow around the aesthetascs and antennules of the real animals must also be used in testing the models. The Reynolds number *Re* is a dimensionless number that represents the ratio of inertial to viscous forces involved in a particular flow situation:

$$Re = (\rho L U)/\mu, \tag{1}$$

where ρ is the density of the fluid (here the density of sea water at 25 °C, $1023 \, \mathrm{kg \, m^{-3}}$), L is a characteristic length (here the diameter of an aesthetasc), U is a velocity (here the velocity of the aesthetascs relative to the surrounding water as an antennule flicks) and μ is the dynamic viscosity of the fluid (here the viscosity of sea water at 25 °C, $0.97 \times 10^{-3} \, \mathrm{Pa \, s}$) (Vogel, 1994). In general, *Re*<1 indicates that viscous forces are dominant and *Re*>1 suggests that inertial forces are important. For a given aesthetasc diameter, a large *Re* indicates that the boundary layer is thin and a small *Re* suggests that the boundary layer is thick relative to *L*. For an object of given *L*, the greater the value of *U*, and therefore of *Re*, the thinner the boundary layer and, hence, the more rapid diffusion of molecules to its surface.

Stomatopod aesthetasc morphology and Reynolds numbers

Stomatopod aesthetascs are located in rows of three on the distal dorsal surface of a filament (termed the aesthetasc filament) that arises from the lateral antennule filament
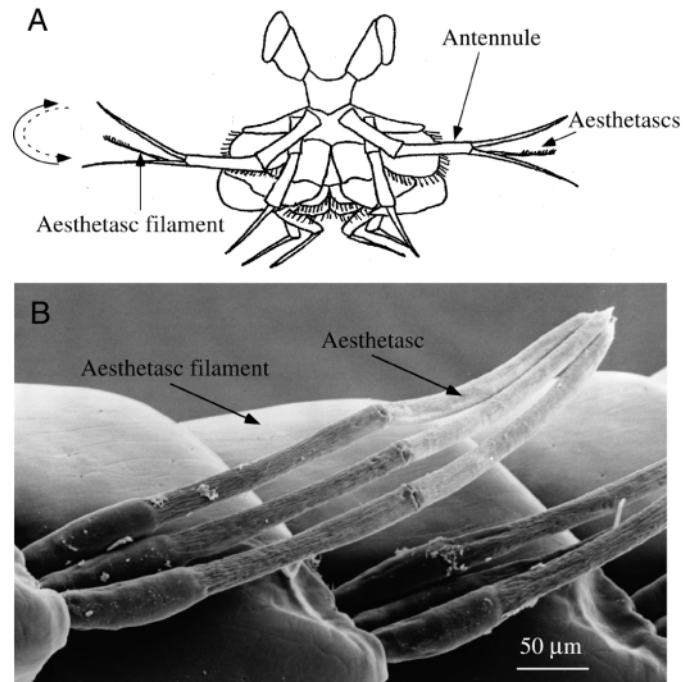

Fig. 1. Stomatopod antennules and aesthetascs. (A) Front view of a stomatopod showing the position of the antennules and the location of the aesthetascs on the antennule filament. The solid arrow indicates the direction of movement (lateral, caudal) of the rapid, outward stroke of an olfactory flick, while the dashed arrow shows the direction (medial, rostral) of the slow return stroke of the flick. (B) Scanning electron micrograph of part of the left aesthetasc-bearing filament of a large adult stomatopod (*Gonodactylaceus mutatus*, 55 mm rostrum–telson length). Scale bar, 50 μm.

(Fig. 1). Thus, the aesthetasc-bearing filament of stomatopods is homologous to the aesthetasc-bearing lateral filament of decapod crustaceans. This arrangement is similar to that of the Malaysian prawn *Macrobrachium rosenbergii* (Hallberg et al., 1992).

As *G. mutatus* grow in rostrum–telson length from 7 to 55 mm, aesthetasc length increases from 150 to 550 μm, aesthetasc diameter increases from 10 to 20 μm and the number of aesthetasc rows increases from three to 18 (Mead et al., 1999). High-speed video analysis has shown that stomatopod olfactory flicks consist of a rapid outward and lateral stroke followed by a medial return stroke at approximately half the velocity of the outward stroke. Over the same range of body sizes, the tangential velocity of the tip of the antennule increases three- to fourfold (Mead et al., 1999). These increases in aesthetasc diameter and antennule velocity with animal size cause the *Re* of the outward stroke to increase from 0.2 to 1.8 and the *Re* of the return stroke to increase from 0.1 to 0.9 (Mead et al., 1999).

Flow between sensilla at aesthetasc Reynolds numbers

One functional consequence of a change in *Re* of a setose appendage can be a change in the leakiness of the setal array. Leakiness is the ratio of the volume of fluid per unit time

Table 1. *Dimensions of juvenile and adult physical models of stomatopod antennules*

	Juvenile animal	Juvenile model	Adult animal	Adult model
Rostrum–telson length (mm)	11		45	
Aesthetasc diameter (mm)	0.01	3.2	0.02	3.2
Aesthetasc length (mm)	0.325	103	0.516	82
Filament diameter (mm)	0.1	32	0.2	32
Number of aesthetasc rows	4	4	16	4
Distance between aesthetascs within a row (mm)	0.01	3.2	0.02	3.2
Segment length (mm)	170	54	170	27
Distance between aesthetascs rows (mm)	0.16	50.8	0.15	23.8
Gap:diameter	10.3	11.3	4.8	5.3
Aesthetasc angle (degrees)	50	45	50	45
Tangential velocity for outstroke (mm s^{-1})	25	8	78	50
Tangential velocity for return stroke (mm s^{-1})	12.3	4	39	25
Re for outstroke	0.27	0.27	1.68	1.68
Re for return stroke	0.13	0.13	0.84	0.84

Re, Reynolds number.

flowing through the gap between adjacent cylinders to the volume of fluid per unit time that would flow through a space of the same width if no cylinders were present (Cheer and Koehl, 1987). Physical and mathematical models (Cheer and Koehl, 1987; Hansen and Tiselius, 1992; Louden et al., 1994; Koehl, 1995, 1996a,b) suggest that, within this *Re* range, a small change in *Re* can result in a large change in the leakiness of an array of sensilla and in the amount of fluid flowing per unit time between adjacent aesthetasc rows.

We used our measurements of aesthetasc gap:diameter ratio with *Re* and leakiness values from Koehl (1995) to estimate the leakiness of stomatopod aesthetasc arrays. These estimates suggest that the flow patterns through stomatopod aesthetasc arrays should be markedly different during the outward stroke and the return stroke of a flick, and in juveniles compared with adults (Mead et al., 1999). The dependence of the changes in flow pattern on flick velocity and animal size suggested that the outward and return motions of the flick might have separate functional roles and that juvenile and adult stomatopods might use different odorant capture strategies to sample their chemical environment. However, the mathematical (Cheer and Koehl, 1987) and physical (Hansen and Tiselius, 1992) models used to generate the graph of leakiness as a function of gap:diameter ratio and *Re* in Koehl (1995) differed in morphology from stomatopod aesthetasc arrays in several ways. The two-dimensional mathematical model of Cheer and Koehl (1987) consisted of two 'infinitely long' cylinders, while the physical model of Hansen and Tiselius (1992) was a comb-like structure. Both models examined flow between cylinders, rather than flow between rows of cylinders, and only the model of Hansen and Tiselius (1992) incorporated the effect of a supporting filament. Furthermore, the range of *Re* that we particularly wished to examine for stomatopods (*Re*=0.1–2.0) was between the *Re* ranges most intensively sampled by the two investigative groups. These discrepancies

led us to create new physical models that more closely resemble stomatopod antennule structure.

The purpose of this study was to use dynamically scaled physical models to measure flow velocity fields through arrays of stomatopod aesthetascs. Our objectives were to use these models (i) to assess the differences in flow through aesthetasc arrays during the outward stroke and return stroke of the flick, (ii) to quantify the hydrodynamic effects of the morphological differences between juvenile and adult antennules, and (iii) to measure the effects of the *Re* change between juvenile and adult antennules.

Materials and methods

Physical models

Because we wanted to study how the flow velocity profile surrounding aesthetascs is affected by animal growth and increases in antennule flicking velocity, we made geometrically scaled physical models of sections of the aesthetasc filaments of antennules from a juvenile (11 mm in rostrum–telson length) and an adult *Gonodactylaceus mutatus* (Lanchester, 1903) (45 mm in rostrum–telson length).

Each model consisted of a section of filament from the left antennule bearing four rows of aesthetascs with three aesthetascs per row. The dimensions of the original antennules and the models are given in Table 1. The models were constructed by wrapping Sculpey modeling compound (S8) around lengths of heat- and pressure-tolerant 0.5 inch (1.27 cm) polyvinylchloride pipe. Aesthetascs made of stainless-steel music wire (3.17 mm diameter; Small Parts Inc. SMW-125-18) were inserted into the Sculpey at an angle of 45 ° (Fig. 2), and the model was baked in an oven for 15 min at 135 °C. Layers of epoxy and silicone were placed around the junction between the aesthetascs and filament to strengthen the structure, and the model was painted black to limit reflection.
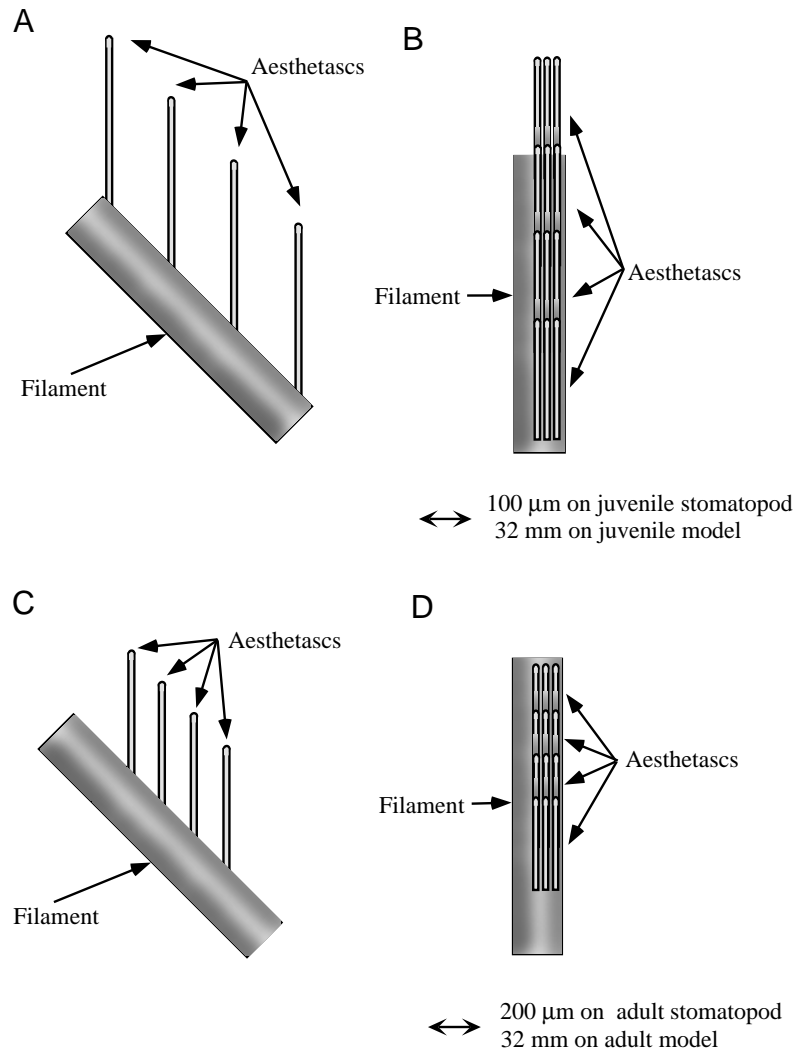
Fig. 2. Diagrams of physical models of a section of the medial antennule filament of juvenile and adult stomatopods (see also Table 1). Both the juvenile and the adult models consist of four rows of three aesthetascs inserted at 45 ° into part of the left antennular filament. (A) Side view of the juvenile model. Aesthetasc and filament measurements were scaled up 317-fold from the mean measurements of a *Gonodactylaceus mutatus* with a rostrum–telson length 11 mm. An animal of this size generally only has four rows of aesthetascs. (B) Top view of the juvenile model. The aesthetascs are placed on the rostral edge of the top part of the filament. This becomes the trailing edge during the outward motion of the flick and the leading edge during the return motion of the flick. Within each row, adjacent aesthetascs are approximately one aesthetasc diameter apart. (C) Side view of the adult model. Aesthetasc and filament measurements were scaled up 159-fold from the mean measurements of *G. mutatus* with a rostrum–telson length of 45 mm. An animal of this size typically bears 16 rows of aesthetascs. (D) Top view of the adult model. Adjacent aesthetascs are approximately one aesthetasc diameter apart.

Experimental arrangement

The towing tank in which we performed our experiments is described by Louden et al. (1994). We carried out our physical model experiments in a 125 l tank (32 cm wide, 46 cm high and 75 cm long) filled with a 3:1 ratio of Karo light corn syrup to distilled water. The density of the diluted Karo syrup was 1280 kg m^{-3}, as measured by weighing a graduated cylinder containing a known volume of the fluid to the nearest 0.1 mg. The viscosity was 0.13 Pa s, measured daily to the nearest 0.002 Pa s with a Brookfield viscometer at 25 °C. We seeded the diluted Karo syrup with *Artemia salina* cysts, which reflected light and were nearly neutrally buoyant, rising at less than 1.5 mm min^{-1}. Since most experiments lasted less than 30 s, most particles remained within the light sheet (3 mm thick) for the duration of the run. The model, oriented such that the filament axis was parallel to the width of the tank and at an angle of 45 ° so that the aesthetascs were vertical, was towed along the long axis of the tank using a Daedal compumotor (LN57-83-MO) controlled by a computer (Texas Instruments TM-5000). This enabled us to determine the *Re* of the model moving through the Karo syrup by controlling the towing speed. We calibrated the towing velocities by making video recordings (at 30 frames s^{-1}) of the motion of the model support structure and digitizing successive frames using NIH image software and a Hotronics, Inc. TBC frame grabber. We created a 3 mm thick horizontal light sheet using two 3 V Imatronic laser diodes (LDM145/670/3/40) with cylindrical lenses. This light sheet intersected the aesthetascs above the filament (Fig. 3). We recorded the motion of the *Artemia salina* cysts with respect to the model aesthetascs (at 30 frames s^{-1}) using a WATEC video camera with a Micro-NIKKOR 55 mm 1:2.8 lens mounted on the support that moved the model through the tank. Images were recorded using a Panasonic VCR (AG-7350).

The tank of dilute Karo syrup was placed in a temperature-controlled room away from windows. Tank volume and temperature were monitored each day to ensure that the density and viscosity of the Karo solution remained constant. The solution in the tank was mixed and the convective movement allowed to die out before each run to ensure an even suspension of marker particles. Although the model was towed from one end of the tank to the other, we made video recordings only when the model was in the center of the tank, minimizing the effects of the end wall (Louden et al., 1994). Digitization of

particle tracks indicated that the flow profiles reached equilibrium well before reaching the section of the tank in which video recordings were made. We tested both the adult and the juvenile models at *Re* values corresponding to an adult flick outward stroke (*Re*=1.68), an adult flick return stroke (*Re*=0.84), a juvenile flick outward stroke (*Re*=0.27) and a juvenile flick return stroke (Re=0.13). *Re* values of 0.065, 0.6 and 1.2 were also tested with both models. Since the aesthetasc diameter was the same on both models, although it represented a 10 μm sensillum in juveniles and a 20 μm sensillum in adults, the juvenile model was towed twice as fast as the adult model to generate a given *Re*. At each *Re*, the model was run 10 times in the direction simulating flick outward stroke and 10 times in the direction of the return stroke. We videotaped overviews, spanning almost the entire width of the tank and showing all four aesthetasc rows, and magnified views showing only 2–3 aesthetasc rows.

Image capture and particle image velocimetry (PIV)

Seventy-six frames of the most well-lit portion of each experimental run were captured and edited to enhance contrast and minimize shadowing using NIH Image. Runs at *Re* values ≤0.27 were sampled at 10 frames s^{-1}, runs at *Re* values of 0.6–1.2 were sampled at 30 frames s^{-1}, and at *Re* values of ≥1.68 the frames were split into individual fields, doubling the maximum effective capture rate to 60 frames s^{-1}. The enhanced images were processed using particle image velocimetry software developed by E. A. Cowen (copyright 1997). This software divided each frame of each run into an array of 'interrogation boxes' and calculated the most probable displacements of particles in successive frames using cross-correlational analysis, as described by Cowen and Monismith (1997). This procedure generates mean and root mean square (rms) velocities for each interrogation box. We used a Mathematica user interface developed by T. Cooper and E. A. Cowen to interpolate mean and rms velocities between the grid points of the interrogation boxes and to display the mean velocities as vector fields (Fig. 4). All 10 trials at each *Re* were pooled to generate one flow field. To facilitate comparison between different experimental conditions, we considered the velocity profiles along a line parallel to the long axis of the filament that intersected the middle aesthetasc of each row, as shown in Fig. 4. These 'slices' display the velocity profiles around the aesthetascs generated as the model moved through the tank of Karo syrup. All data presented are converted to the velocities that would be experienced near aesthetascs of the dimensions of real stomatopod aesthetascs operating at the *Re* values of the experiment.

Velocity gradient measurement

Velocity gradients were measured by calculating the mean of the maximum slopes of the velocity profiles to the right of the aesthetascs in rows 2 and 3. The profiles to the left of the aesthetascs were not considered because these regions were slightly shadowed, resulting in larger errors. Since row 4 is on the edge of the array and thus experienced a different flow field, its velocity profiles were also disregarded.
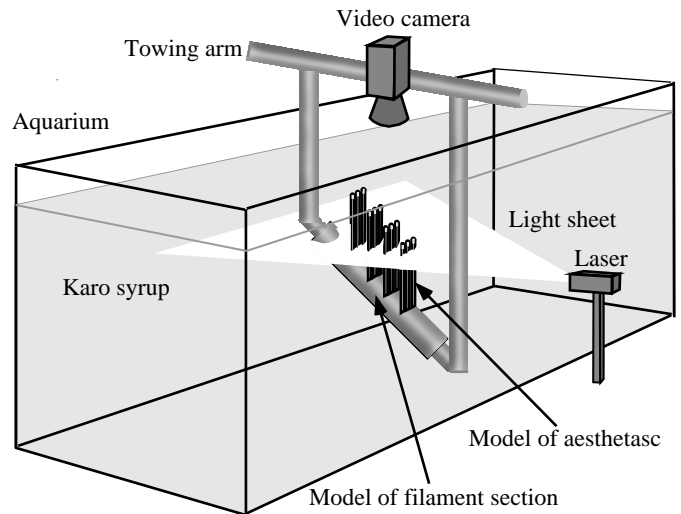

Fig. 3. Experimental arrangement. The physical model (here, the adult version) is suspended in a tank of diluted Karo syrup and is towed by a computer-driven motor (not shown) along the long axis of the tank. A laser illuminates a thin, horizontal sheet of light that intersects the aesthetascs and reflects off neutrally buoyant particles suspended in the fluid. The movement of these lit particles through the aesthetasc array is recorded by a camera that moves with the model.

Calculation of leakiness and flow rate

Leakiness *A* was calculated by integrating the measured velocity profile between two aesthetascs and dividing that by the product of gap width and antennule freestream velocity. The volume rate of fluid flow (*F*) between two adjacent aesthetasc rows was calculated using the following equation:

$$F = L_a L_g VA \sin\alpha, \qquad (2)$$

where L_a is the aesthetasc length, L_g is the distance (gap) between adjacent rows of aesthetascs, *V* is the velocity at which the model was towed in the tank, and α is the angle at which the aesthetascs are inserted into the antennule filament. We used an average of the leakinesses between rows 2–3 and rows 3–4 in this equation. We also calculated the volume rate of fluid flow through the entire aesthetasc array, extending (in the adult) beyond the model, as if the juvenile bore four rows of aesthetascs and the adult 16 (Table 1).

Statistical analysis of PIV data

We compared mean velocities, leakinesses and volume flow rates using a minimum-significant-difference statistic that is a composite of the standard error and the critical value of the studentized range Q_{crit} (Sokal and Rohlf, 1995). Although between 100 and 300 particle displacements were calculated per interrogation box per experiment (a set of 10 measurements at a given *Re*), we were concerned that not all of these particle displacements represented independent measurements. Therefore, we conservatively used only the number of times each model was run at a given *Re* in a given direction (10) as *N* when calculating the standard error and in choosing Q_{crit}.

A

Side view

Aesthetascs

Filament

Light sheet

Top view

Velocity profile

B

Velocity (cm s^{-1})

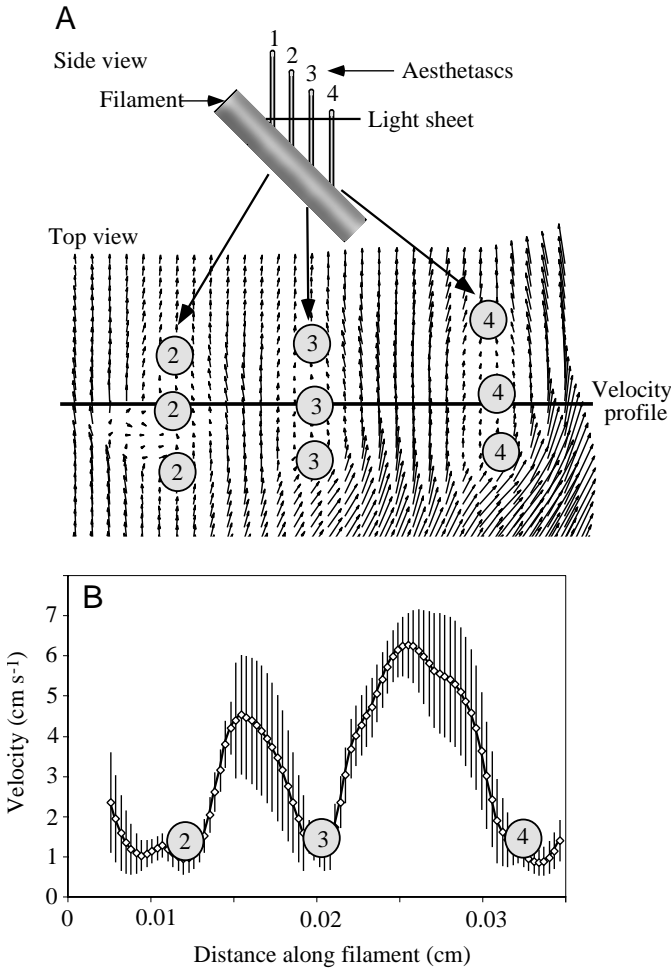Distance along filament (cm)

Fig. 4. Vector field output from particle image velocimetry (PIV). (A) In this diagram (and in Figs 5, 6, 12 and 13), the grey circles indicate aesthetasc position and (by number) location on the filament. The length of an arrow is proportional to the velocity at the tail of that arrow. Since the light sheet is horizontal and the model is at an angle, the light sheet intersects row 4 near the aesthetasc tip, row 3 in the middle of the aesthetasc and row 2 near the base of the aesthetasc. Note that the velocity is greater near the aesthetasc tip than near the aesthetasc base. The thick horizontal line following the long axis of the antennule filament shows the location of the velocity profile taken to compare data sets. (B) The velocity profile shown in A. The velocities are plotted as a function of position along the line through the flow field indicated by 'velocity profile' in A. Values are means $\pm \frac{1}{2}$ mean significant differences; $N=10$. Note that the error bars are greater to the left of the aesthetascs than to their right because the lighting scheme employed cast intermittent shadows to the left of the aesthetascs so that fewer tracer particles were illuminated.

corresponding velocity profiles of an adult stomatopod are shown in Fig. 6. The overall flow patterns of the outward and return strokes are similar: the velocity is low near the aesthetascs and rises to a peak midway between adjacent aesthetasc rows. In both juveniles and adults, the maximum mean velocity of the fluid moving through the aesthetasc array during the outward stroke of a flick is 3–6 times greater than during the return stroke, although the freestream velocities of the two parts of the flick (U_{out} and U_{return}) differ only by a factor of 2.

In both the juvenile and the adult, the ratio of the maximum mean velocity between aesthetasc rows to the freestream velocity is greater on the outward stroke than on the return stroke, and the slopes of the velocity profiles are greater on the outward stroke than on the return stroke (Figs 5, 6).

The leakiness of adjacent aesthetasc rows in stomatopod aesthetasc arrays is affected by aesthetasc Re, by the morphology of the aesthetasc array and by the position along the aesthetasc (Fig. 7). Because the velocity of the outward

Results

Flow through aesthetasc arrays during olfactory flicking: the outward stroke versus *the return stroke*

Velocity profiles from the outward and return strokes of a flick of a juvenile stomatopod are shown in Fig. 5, and the

Fig. 5. Velocity profiles from an olfactory flick of the antennule of a juvenile. The velocities are plotted as a function of position along the line through the flow field indicated by 'light sheet' on the diagram. Filled diamonds show flow velocities through the aesthetasc array during the rapid outward stroke of a flick, and filled squares show flow velocities during the return part of the flick. The freestream velocity (i.e. antennule speed) during the outward stroke is indicated by U_{out}; the freestream velocity during the return stroke is U_{return}. Values are means $\pm \frac{1}{2}$ mean significant differences; $N=10$. The horizontal line on the model shows the position of the light sheet. All velocities and spatial distances are reported for an antennule the size of a real antennule rather than for one the size of the model. The grey circles indicate aesthetasc position and (by number) location on the filament.

Velocity (cm s^{-1})

Distance along filament (cm)
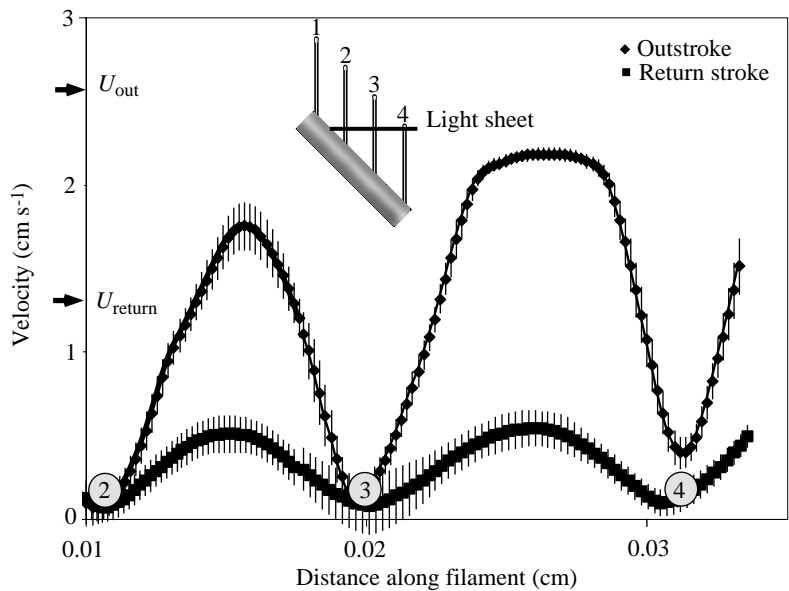
◆ Outstroke
■ Return stroke

Light sheet

Fig. 6. Velocity profiles for an olfactory flick by an adult antennule. The velocities are plotted as a function of position along the line through the flow field indicated by 'light sheet' on the diagram. Open diamonds show flow velocity through the aesthetasc array during the rapid outward stroke of a flick and open squares show flow velocity during the return part of the flick. The mainstream velocity during the outward stroke is indicated by U_{out}; the mainstream velocity during the return stroke is U_{return}. Values are means $\pm$ $\frac{1}{2}$ mean significant differences; $N=10$. The grey circles indicate aesthetasc position and (by number) location on the filament.
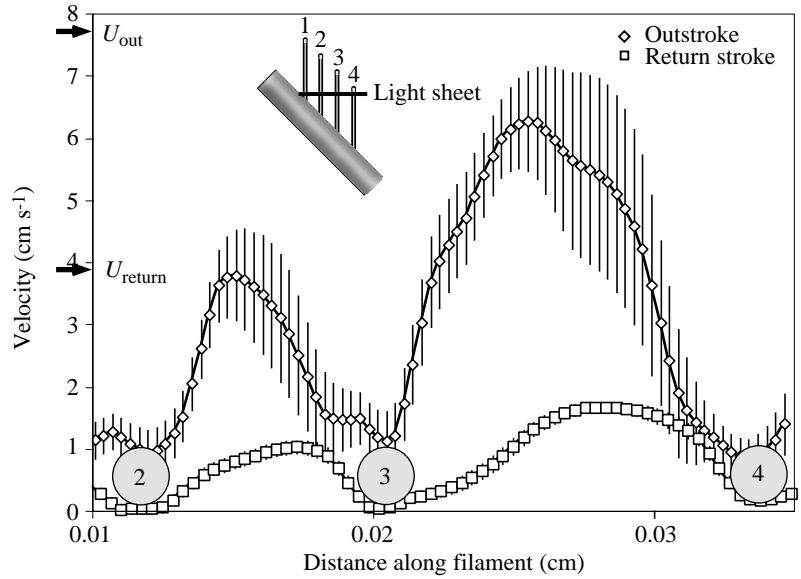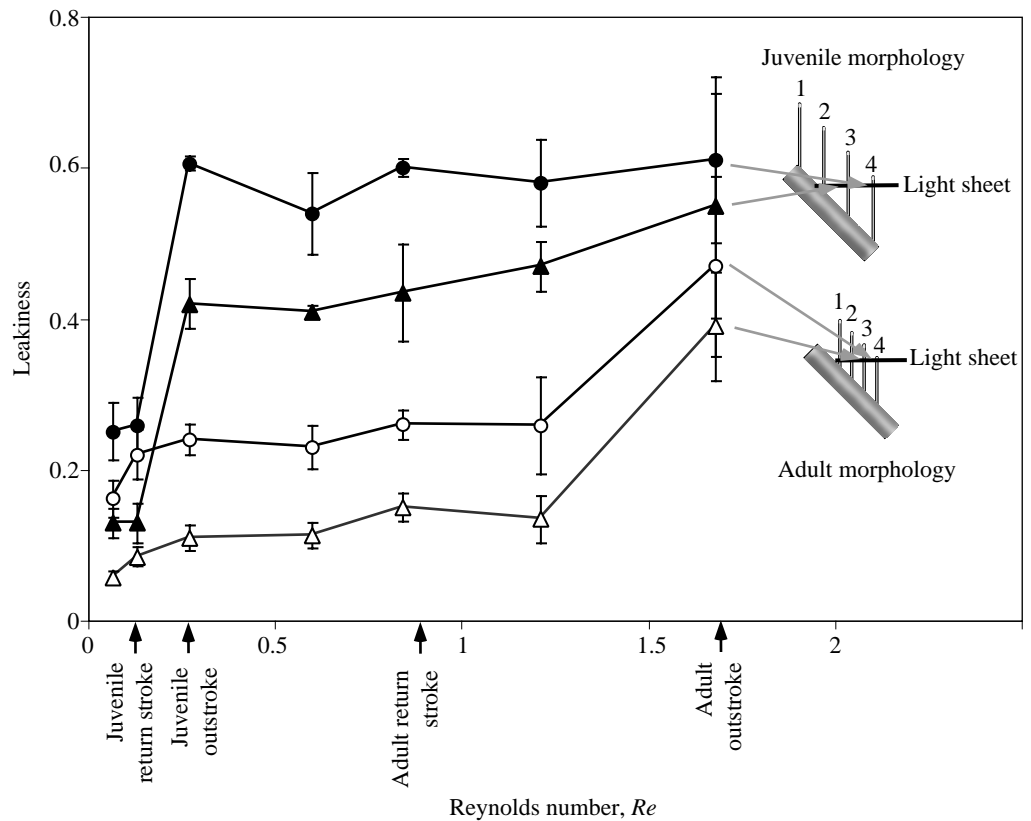

Fig. 7. The effects of aesthetasc Reynolds number Re on leakiness. Filled symbols refer to the leakiness of the juvenile model, open symbols to the adult model. In both cases, circles refer to the leakiness between rows 3 and 4, and triangles to the leakiness between rows 2 and 3. Values are means $\pm$ $\frac{1}{2}$ mean significant differences; $N=10$.

stroke of a flick is twice as great as the velocity of the return stroke, the leakiness of the two parts of a flick differs. For an animal of a given size, the leakiness of the outward stroke is always greater than the leakiness of the return stroke (Fig. 8). At their operational Re values ($Re_{out}=0.27$, $Re_{return}=0.13$), the ratio of juvenile outward stroke to return stroke leakiness is 2.3–3.2, depending on the distance from the filament (Fig. 9A). At lower Re values, the leakiness ratio is approximately 1 because both leakinesses are low; at higher Re values, the leakiness ratio is approximately 1 because both leakinesses are high. Adults also maximize the leakiness ratio of the outward and return strokes at their operational Re values ($Re_{out}=1.68$, $Re_{return}=0.84$) (Fig. 9B). Therefore, both juvenile and adult stomatopods operate their antennules at Re values that maximize the difference in leakiness between the outward and return strokes of a flick. The higher antennule velocity and

Fig. 8. The effects of body size, flick stroke and aesthetasc position on leakiness. Black and light grey columns indicate, respectively, the leakiness during the outward stroke and return stroke on the proximal portion of the aesthetasc, and dark grey and white columns show the leakiness during the outward stroke and return stroke, respectively, on the distal region of the aesthetasc. Values are means $\pm \frac{1}{2}$ mean significant differences; $N=10$.
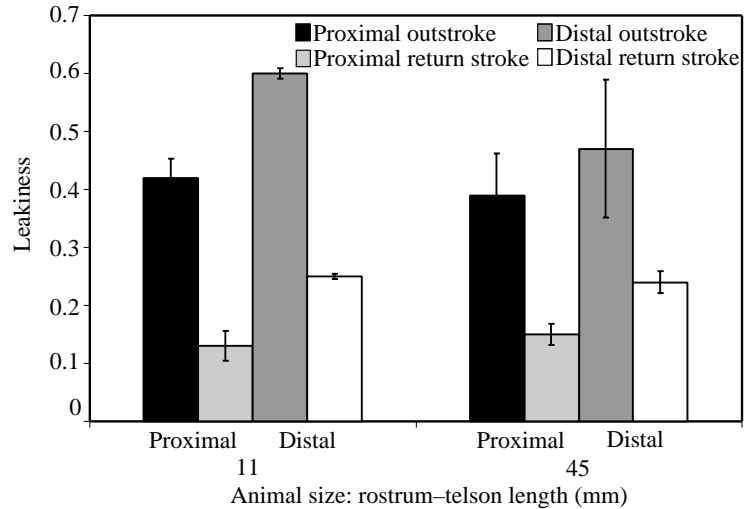
leakiness during the outward stroke of the flick create volume flow rates between adjacent aesthetasc rows that are four times greater during the outward stroke than during the return stroke (Fig. 10A). The volume flow rate between all the rows of the aesthetasc array (four for the juvenile, 16 for the adult) is nearly four times greater during the outward stroke than during the return stroke (Fig. 10B). Both adults and juveniles flick at Re values that maximize the ratio of the outward stroke to return stroke flow rates for their antennule morphologies (Fig. 11).

Flow through aesthetasc arrays of juveniles versus adults

Both antennule velocity and gap:diameter ratio change with body size (Table 1) and affect leakiness. Adults flick their antennules more quickly and at a higher Re than juveniles, so the maximum velocity of the fluid moving through the aesthetasc array is correspondingly faster and the velocity gradients are steeper (Figs 5, 6). The increase in leakiness due to the rise in antennule velocity is counteracted by the decrease in leakiness caused by the fall in gap:diameter ratio (from 11.3 to 5.3) such that leakiness is held constant over a large range of animal sizes (Fig. 8). Changes in aesthetasc length and antennule velocity result in four times as much fluid per unit time flowing between adjacent rows of sensilla in adults as in juveniles (Fig. 10A). Since adult antennules bear several times more rows of aesthetascs than juvenile antennules, nearly 20 times more fluid penetrates adult arrays than juvenile arrays during both the outward stroke and the return stroke (Fig. 10B).

Effects of changes in antennule geometry during ontogeny on flow

The antennules of *G. mutatus* grow allometrically: since aesthetascs grow wider as the animal grows larger, the rows of sensilla are more closely spaced relative to aesthetasc diameter on adults than they are on juveniles. If stomatopods maintained the juvenile antennule geometry of thin, widely spaced aesthetascs while operating at an adult Re, then the peak water velocity between rows of aesthetascs during the outward stroke

of a flick would be 2–3 times greater than it is for the adult geometry, and velocity gradients near the aesthetascs would more than double (Fig. 12A). Because the return stroke would become nearly as leaky as the outward stroke, the ratio of outward stroke to return stroke leakiness would fall to near 1 (Fig. 9), and the flow rate ratio of the outward stroke to the return stroke would decrease (Fig. 11).

If stomatopods started life with the adult antennule geometry (i.e. thick aesthetascs in closely spaced rows) but operated at their customary juvenile Re, then the peak water velocity between adjacent aesthetasc rows during the outward stroke of a flick would be approximately six times less than it is for the juvenile geometry, and velocity gradients would be more gentle (Fig. 12B). Outward stroke leakiness would decrease more than return stroke leakiness, so that the leakiness ratio of the two strokes would fall to 1 (Fig. 9), and the flow rate ratio of the outward stroke to the return stroke would also decrease (Fig. 11).

Effects of changes in aesthetasc Re during ontogeny on flow

The Re values describing the motion of aesthetascs through the surrounding fluid during olfactory sampling increase approximately sixfold from 0.13–0.27 (juvenile return stroke, outward stroke) to 0.84–1.68 (adult return stroke, outward stroke) as stomatopods grow from 11 to 45 mm in rostrum–telson length (Mead et al., 1999). If stomatopods did not increase their flicking Re values as they grew, peak velocities, velocity gradients and flow rates between aesthetasc rows would be approximately 20 times less than normal (Fig. 13A), and the ratios of outward stroke to return stroke leakiness and of outward stroke to return stroke flow rate would fall (Figs 9, 11). If stomatopods operated at adult Re values throughout their life histories, juvenile animals would be exposed to steeper velocity gradients, would have leakier aesthetascs and would process a greater volume of fluid per second. The ratios of both the outward to return stroke leakiness and volume flow rate would decrease.

Spatial distribution of flow on aesthetascs

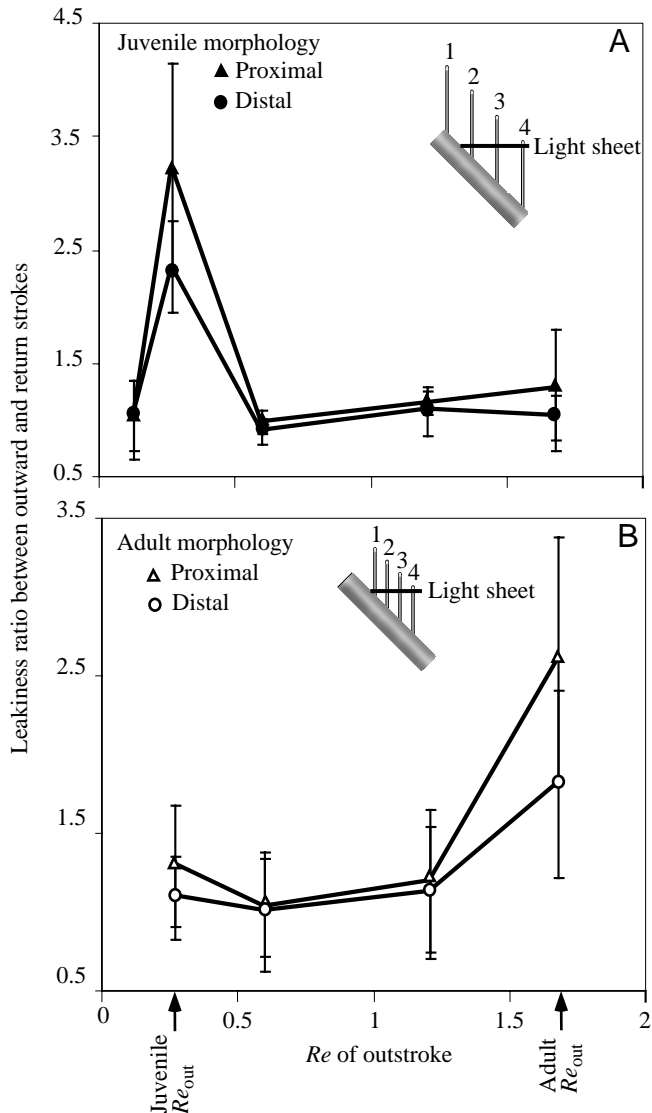In both juveniles and adults, the peak fluid velocity is

Fig. 9. Reynolds number *Re* and the leakiness ratio between the outward and return strokes of a flick. (A) Juvenile. (B) Adult. Leakiness ratios are plotted against the *Re* of the outward stroke (*Re*out) of a flick. In both A and B, circles refer to the leakiness between rows 3 and 4, and triangles to the leakiness between rows 2 and 3. Values are means $\pm \frac{1}{2}$ mean significant differences; *N*=10.
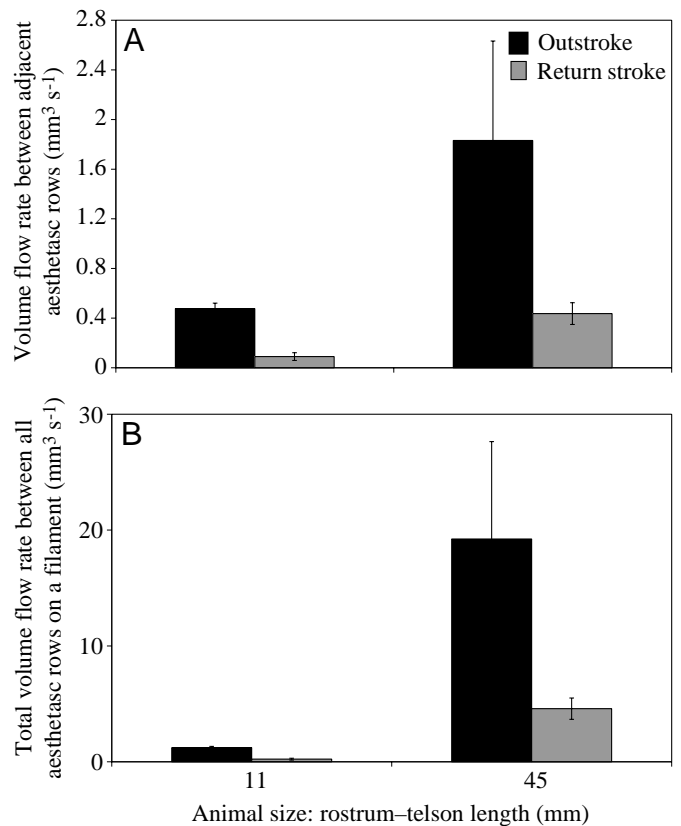

Fig. 10. Volume flow rate through the aesthetasc array (A) between one pair of adjacent aesthetasc rows and (B) between all the aesthetasc rows of the array (four for the juvenile, 16 for the adult). Volume flow rates per second are plotted against stomatopod rostrum–telson length. Black columns indicate the outward stroke of the flick and grey columns show the return stroke. Values are means $\pm \frac{1}{2}$ mean significant differences; *N*=10.

greater near the aesthetasc tips than close to the aesthetasc bases (Figs 5, 6). Thus, leakiness between rows at a particular *Re* or for an animal of a given size is greater near the tips of the aesthetascs than near their bases (Figs 7, 8). This effect is particularly pronounced in adults moving at low *Re* values (Fig. 7). As a result, flow rate is greater near the aesthetasc tips than near the sensillar bases. This effect of aesthetasc position on fluid velocity, leakiness and flow rate is due to the formation of a boundary layer around the antennule filament to which the aesthetascs are attached. Near the base of the aesthetasc, this boundary layer affects flow. Farther away from the filament, the effect of its boundary layer is minimal.

Discussion

Asymmetry of the olfactory flick

Although their antennule morphologies are quite different, both juvenile and adult stomatopods flick their antennules with *Re* values that maximize the difference in leakiness between the fast outward stroke and the slow return stroke of a flick (Fig. 9). This result is consistent with the prediction of the model of Cheer and Koehl (1987) that, when the gap to diameter ratio decreases, the transition from low leakiness to high leakiness occurs at a higher *Re*. The differences in leakiness and in antennule velocity enable four times as much fluid (and any odorants in the fluid) to penetrate the aesthetasc array per second during the outward stroke as during the return stroke (Fig. 10).

One consequence of this difference in flow rate is that the water surrounding the aesthetascs at the end of a flick is different from the water surrounding them before the flick, ensuring discrete sampling of odor signals (see also Mead and Koehl, 1999; J. Goldman and M. A. R. Koehl, unpublished data). The fact that both juvenile and adult stomatopods use their antennules in a way that maximizes the difference in flow
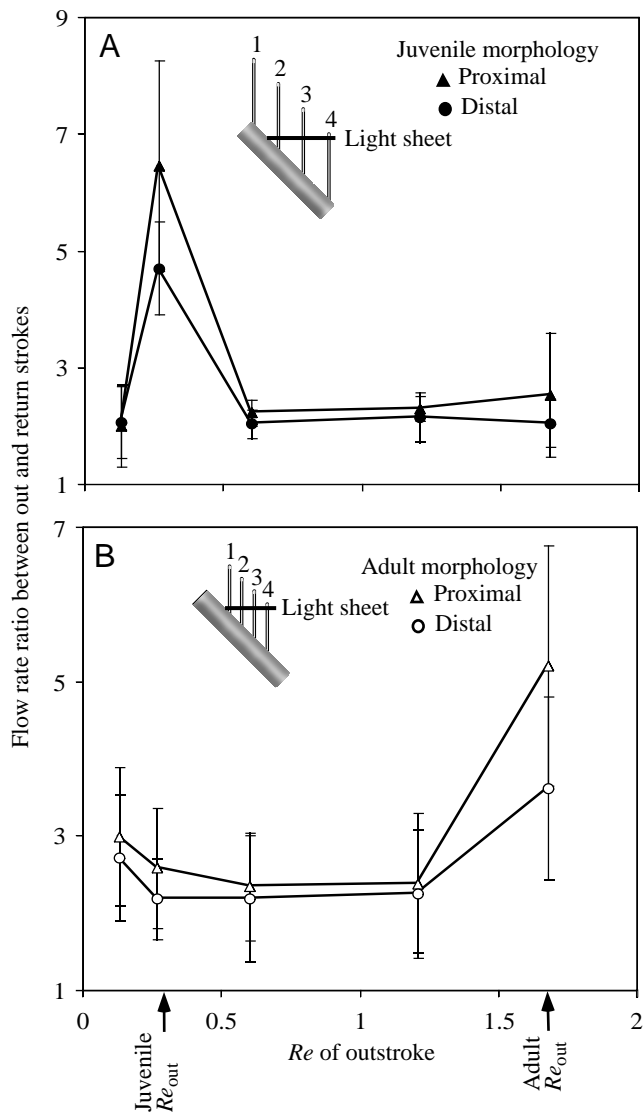
Fig. 11. Reynolds number Re and the ratio of volume flow rates between the outward and return strokes of a flick. (A) Juvenile. (B) Adult. Flow rate ratios are plotted against the Re of the outward stroke (Re_{out}) of a flick. In both A and B, circles refer to the leakiness between rows 3 and 4, and triangles to the leakiness between rows 2 and 3. Values are means $\pm \frac{1}{2}$ mean significant differences; $N=10$.

rate between the two strokes of a flick suggests that pulsatile sampling is functionally important.

A second consequence of the asymmetries of the flick is that the velocity gradients close to the aesthetascs are steeper on the outward stroke than on the return stroke. When flow rates through a sensillar array are high and velocity gradients are steep, newly sampled fluid penetrates near to the aesthetasc surface. Odor molecules only have to diffuse a short distance, and the number of molecules captured per unit time by the sensilla is relatively high (e.g. Shimeta and Jumars, 1991; Koehl, 1996a). Less time is therefore needed for odorants to diffuse to the aesthetasc during the fast outward stroke than during the slow return stroke.

Juvenile and adult olfactory strategies

The differences in flow patterns around juvenile and adult aesthetascs may have functional consequences. The fourfold higher flow rate through adjacent aesthetasc rows of large stomatopods should enable them to shed 'old' water from their antennules more quickly and completely than small animals can (Fig. 10A), enhancing their ability to take temporally and spatially discrete samples. The high flow rate and steep velocity gradients near the adult aesthetascs enable odorants to diffuse to adult aesthetasc surfaces more rapidly than to juvenile ones. Exposure to rapid flow also increases the molecule encounter rate of the sensillar array (Shimeta, 1993; Koehl, 1996a). Rapid odorant access increases the ability of the adult animals to respond quickly to the environment and makes them potentially more sensitive than small animals to changes in odorant concentration.

In contrast, the relatively low volume flow rates and gentle velocity gradients near juvenile mantis shrimp aesthetasc arrays may mean that the number of odorant molecules captured per unit time is low. The longer time required for odorant molecules to diffuse to the aesthetasc surface is likely to limit the ability of the juvenile to detect rapid changes in odorant concentration. However, the slower the flow through the sensillar array, the greater the probability that an odorant molecule in the fluid will have time to diffuse to the surface of the array. Since odor filaments move through the juvenile array more slowly (because juveniles flick more slowly) than through the adult array, juvenile sensilla may capture a larger proportion of the odor molecules in a sample even though the capture rate is low (e.g. Rubenstein and Koehl, 1977; Koehl, 1996a).

If capture rates of odorant molecules are low for juvenile stomatopods, we might expect the animal to allow more time to pass after a flick before flicking again, to maximize the information gathered per 'sniff'. This may be reflected in the fact that the maximum flicking frequency during a burst of flicking increases with animal size, from 2 flicks s^{-1} for an animal with rostrum–telson length 11 mm to 7 flicks s^{-1} for a 55 mm animal (Mead et al., 1999).

This change in odor sampling strategy from a juvenile approach favoring less frequent, slow flicks that capture a high proportion of molecules slowly to an adult approach enabling frequent, rapid odorant access to aesthetascs correlates with changes in the ecology and behavior of the animal. While collecting in the field, we noticed that, although juvenile and adult *G. mutatus* live in the same flow environment (oscillatory flow with a peak velocity of 15 cm s^{-1} at 2 cm above the substratum; M. A. R. Koehl and T. Cooper, unpublished data), they occupy different microhabitats. Juvenile *G. mutatus* live in crevices on the coral rubble surface, are not territorial, eat slow-moving prey, do not mate and may not, therefore, need to sample odorants quickly or frequently (Caldwell et al., 1989; Mead et al., 1999). Adult *G. mutatus* occupy burrows in coral rubble. As stomatopods grow, competition for burrows and mates becomes more important, and the speed of their preferred prey increases. Since many of these interactions rely on the rapid gathering
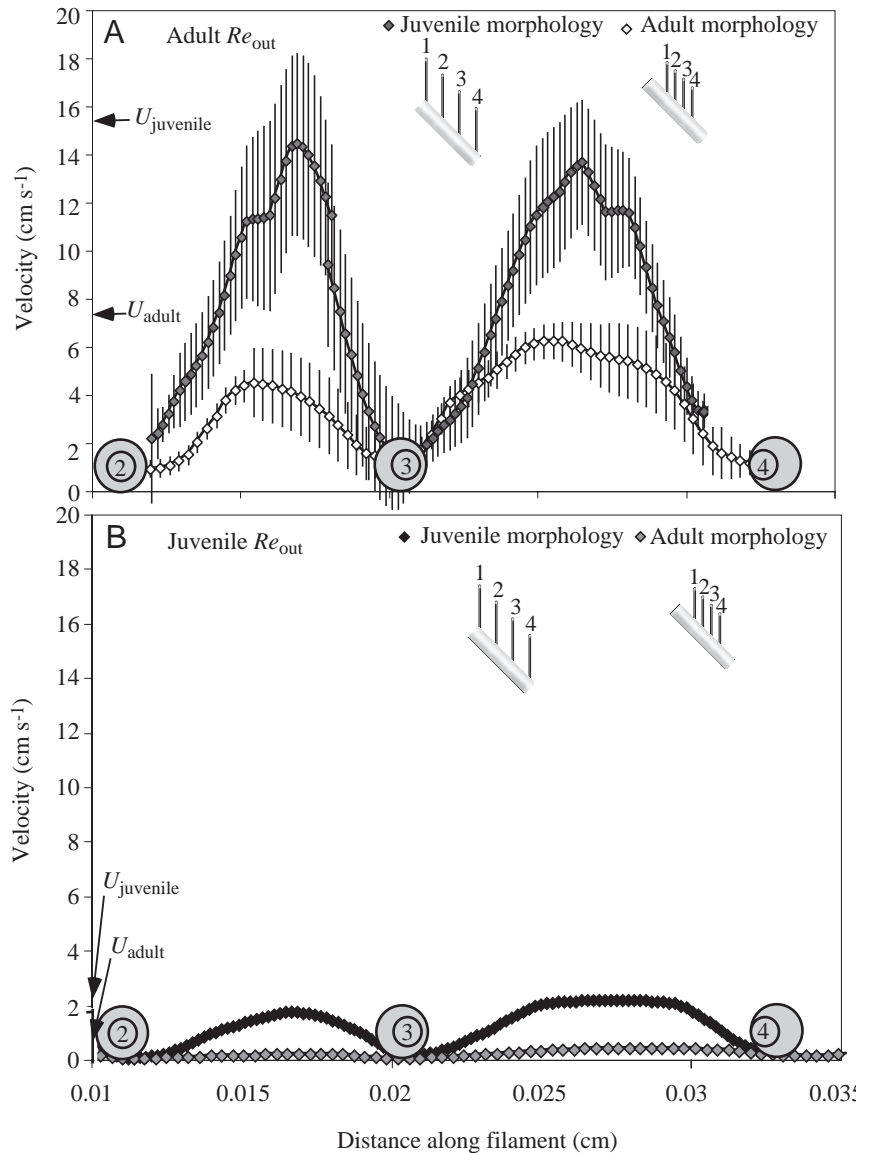
Fig. 12. The importance of the size-dependent changes in aesthetasc and antennule morphology on flow patterns. (A) Adult outward stroke Reynolds number Re_{out}. Shaded diamonds show the flow velocity through the aesthetasc array during the outward stroke of a flick by a juvenile stomatopod operating at an adult Re (the flow pattern if aesthetascs maintained juvenile morphology throughout their life history). Open diamonds show the flow velocity through the aesthetasc array during the outward stroke of a flick by an adult stomatopod operating at an adult Re (normal situation). (B) Juvenile outward stroke Re. Black diamonds show the flow velocity through the aesthetasc array during the outward stroke of a flick by a juvenile stomatopod operating at the juvenile Re (normal situation). Grey diamonds show the flow velocity through the aesthetasc array during the outward stroke of a flick by an adult stomatopod operating at a juvenile Re (the flow pattern if aesthetascs start off with the adult morphology and maintain it throughout the life history). Small grey circles refer to the juvenile aesthetasc position, large circles refer to that of the adult. Values are means $\pm \frac{1}{2}$ mean significant differences; $N=10$. Error bars in B are within the symbols. $U_{juvenile}$ and U_{adult} refer to the mainstream velocities during the outward stroke of the juvenile and adult models respectively.

of olfactory information *via* the aesthetascs (Caldwell et al., 1989), adults may need to facilitate odorant access by flicking their antennules faster and more frequently than juveniles (Mead et al., 1999).

Consequences of ontogenetic changes in antennule morphology

The changes in antennule morphology that occur as the animals grow (an increase in aesthetasc length and diameter, and a decrease in aesthetasc gap:diameter ratio) help to keep leakiness constant and sampling pulsatile throughout the life history of the animal. Thus, the transition in leakiness between the outward stroke and the return stroke occurs at low Re pairs (i.e. $Re_{out}=0.27$, $Re_{return}=0.13$) for the juvenile morphology and at high Re pairs for the adult morphology ($Re_{out}=1.68$, $Re_{return}=0.84$). The morphological changes also affect the volume flow rate and the steepness of the velocity gradient near the aesthetasc, which both increase with body size, resulting in

faster odorant access for adults but possibly higher odorant capture percentages for juveniles.

Our models suggest that animals flicking with Re values different from their operational Re pairs would experience a smaller difference in leakiness and volume flow rate through the aesthetasc array between the outward stroke and return stroke and would therefore be less efficient at replacing previously sampled fluid with new fluid. Pulsatile sampling permits small volumes of water discrete in space and time to be sampled. Such information would be unavailable to animals that cannot efficiently clear their aesthetasc array of previously sampled water.

Mismatched antennules and flicking Re values may also result in different odor sensitivities. If a stomatopod maintained juvenile morphology while flicking at an adult Re, the steeper velocity gradients would speed up odorant access to the aesthetasc. But the enhanced leakiness and volume flow rate would cause the odor filament to move
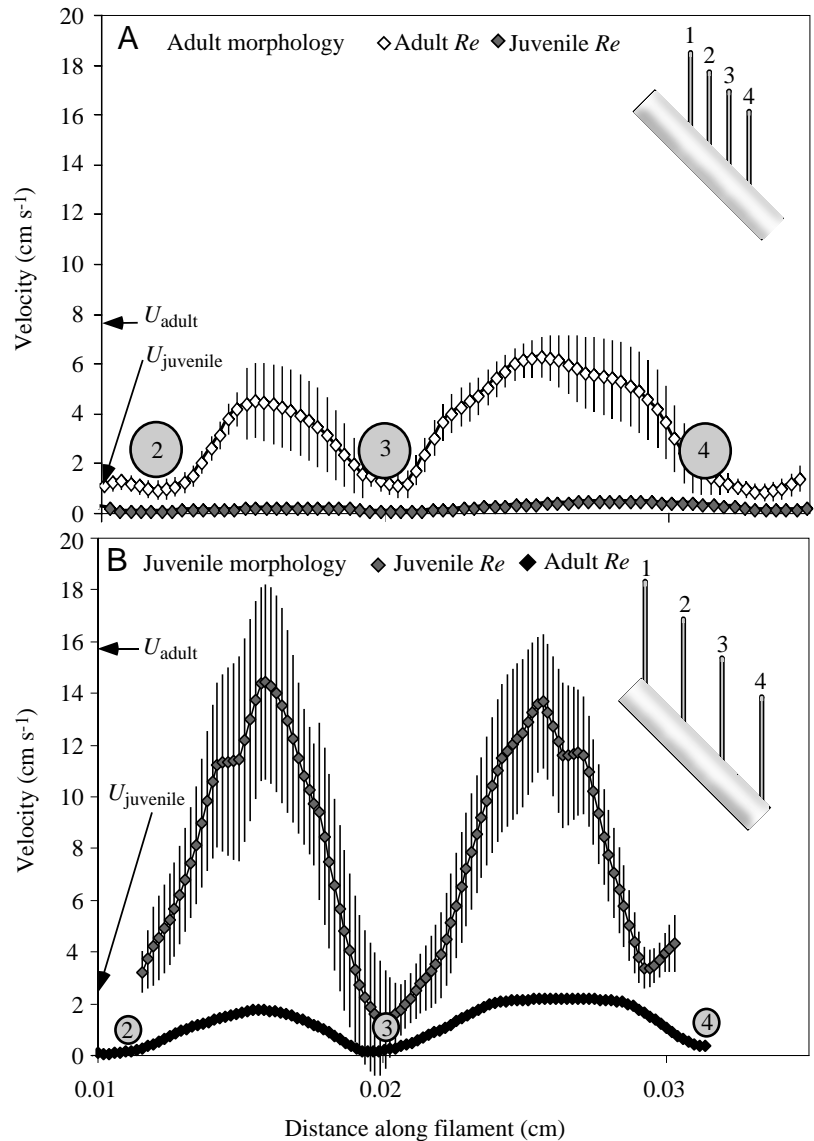
Fig. 13. The importance of size-dependent velocity changes on flow through the aesthetasc array. (A) Adult morphology. Open diamonds represent the flow velocity through the aesthetasc array when the model operates at the adult flick outward stroke Reynolds number Re. Grey diamonds indicate the flow velocity of the model operating at the Re of a juvenile flick outward stroke, indicating the flow pattern that would result if Re did not increase with body size. (B) Juvenile morphology. Grey diamonds represent the flow velocity through the aesthetasc array of the juvenile model operating at the adult Re for a flick outward stroke. Black diamonds indicate the flow velocity of the juvenile model operating at the Re of a juvenile flick outward stroke. $U_{juvenile}$ and U_{adult} refer to the mainstream velocities during the outward stroke of the juvenile and adult models respectively. Values are means $\pm \frac{1}{2}$ mean significant differences; $N=10$. Grey circles indicate the position of the aesthetasc.

through the array more quickly than normal. This might decrease the percentage of odor molecules that would have time to diffuse across the boundary layer to the aesthetasc surface before the odor filament was swept away. If chemoreceptors, by analogy with photoreceptors (Barlow, 1958; Hood and Grover, 1974), require that a threshold number of odor molecules bind to trigger a response, the ability of the animal to detect transient, low-concentration odors might decrease.

Animals that flicked at a juvenile Re while bearing the adult antennule morphology would experience almost no fluid penetration of the aesthetasc array. The very low leakiness and shallow velocity gradients would slow odorant delivery to the aesthetasc surface and, therefore, hamper the ability of the stomatopod to sample its chemical environment.

These manufactured cases of stomatopod antennule design and operation emphasize the potential trade-off between rapid odorant access and high percentages of molecular capture. They indicate how antennules operating at inappropriate Re

values might lose sensitivity to transient odor signals, raising the possibility that antennules, like odor receptors (Gomez et al., 1999), may be tuned to the properties of odor filaments characteristic of their environment.

The focus of this paper is on the arrival of molecules at the surface of the aesthetasc. Many other processes must ensue (diffusion through the cuticle, the lumen and on the surface of the outer dendritic segments) before binding to an olfactory receptor occurs and the cascade of events leading to olfactory neural output begins. These processes are also likely to scale as a function of size. For example, since the average time required for a molecule to diffuse across a particular distance is proportional to the square of that distance, diffusion times within the aesthetasc will probably be longer for adults than for juveniles. However, it is likely that adult aesthetascs contain more sensory cells than juvenile sensilla, as is the case in the prawn *Macrobrachium rosenbergii* (Hallberg et al., 1997) and the crayfish *Cherax destructor* (Sandeman et al., 1998). Similarly, insight into where stomatopod olfactory

receptors fall within the spectrum of concentration or flux detectors (Kaissling, 1998a,b; Gomez et al., 1999; Rospars et al., 2000) will help us interpret the changes in molecular arrival at the sensillar surface as a function of flick stroke and animal size. Taken together, information about the scaling of exterior and interior events will give us an understanding of how a stomatopod's perception of its olfactory environment scales with size.

Spatial distribution of flow on aesthetascs

The fact that the leakiness is greater and the volume fluid flow rate is faster near aesthetascs tips than near their bases suggests that odorant access to the aesthetasc surface will be more rapid distally than proximally. The relatively large flow rate ratio near the aesthetasc tips indicates that old odor is flushed out and new odor sampled most efficiently at the aesthetasc tips. This outer portion of the aesthetasc is the region that contains the outer dendritic segments (K. S. Mead and T. M. Weatherby, unpublished observations), which is where the chemoreceptors are thought to reside. Although juvenile aesthetascs are shorter than adult aesthetascs, they are disproportionately longer relative to the filament diameter (Mead et al., 1999). This morphological feature projects the outer-dendritic-segment-containing region of the aesthetasc into faster flow, facilitating odorant access.

Stomatopod antennule design

Our experiments demonstrate the importance of antennule design. They show that, when operated at the correct *Re*, both juvenile and adult antennules allow different volumes of fluid to flow through the sensillar array during the two strokes of the flick, ensuring pulsatile, and thus efficient, olfactory sampling. In contrast, antennules with mismatched *Re* values (models) do not sample discretely and may not be as sensitive to transient odors as antennules on real animals. The efficiency of the stomatopod antennule design is also apparent in the high concentration of olfactory neuron outer dendritic segments in the part of the aesthetasc that experiences the steepest velocity gradient, the highest volume flow rate and the greatest outward to return stroke flow rate ratio.

References

Ache, B. W. (1982). Chemoreception and thermoreception. In *The Biology of Crustacea*, vol. 3 (ed. H. L. Atwood and D. C. Sandeman), pp. 369–393. New York: Academic Press.

Atema, J. and Voigt, R. (1995). Behavior and sensory biology. *In Biology of the Lobster* Homarus americanus (ed. J. R. Factor), pp. 313–348. San Diego: Academic Press.

Barlow, H. B. (1958). Temporal and spatial summation in human vision at different background intensities. *J. Physiol., Lond.* **141**, 337–350.

Best, B. (1995). Scaling and flow dynamics of crustacean antennules: What's flicking all about? *Am. Zool.* **35**, 53A.

Caldwell, R. L. (1979). Cavity occupation and defensive behaviour in the stomatopod *Gonodactylus festae*: evidence for chemically mediated individual recognition. *Anim. Behav.* **27**, 194–201.

Caldwell, R. L. (1985). A test of individual recognition in the stomatopod *Gonodactylus festae*. *Anim. Behav.* **33**, 101–106.

Caldwell, R. L. (1987). Assessment strategies in stomatopods. *Bull. Mar. Sci.* **41**, 135–150.

Caldwell, R. L. (1992). Recognition, signalling and reduced aggression between former mates in a stomatopod. *Anim. Behav.* **44**, 11–19.

Caldwell, R. L., Roderick, G. K. and Shuster, S. M. (1989). Studies of predation by *Gonodactylus bredini*. In *Biology of Stomatopods. Collana UZI, Selected Symposia and Monographs* (ed. E. A. Ferrero), pp. 117–131. Modena: Mucchi Editore.

Cheer, A. Y. L. and Koehl, M. A. R. (1987). Paddles and rakes: fluid flow through bristled appendages of small organisms. *J. Theor. Biol.* **129**, 17–39.

Cowen, E. A. and Monismith, S. G. (1997). A hybrid digital particle tracking velocimetry technique. *Exp. Fluids* **22**, 199–211.

Derby, C. D. (1982). Structure and function of cuticular sensilla of the lobster *Homarus americanus*. *J. Crust. Biol.* **2**, 1–21.

Derby, C. D., Cate, H. S. and Gentilcore, L. R. (1997). Perireception in olfaction: molecular mass sieving by aesthetasc sensillar cuticle determines odorant access to receptor sites in the Caribbean spiny lobster *Panulirus argus*. *J. Exp. Biol.* **200**, 2073–2081.

Devine, D. V. and Atema, J. (1982). Function of chemoreceptor organs in spatial orientation of the lobster, *Homarus americanus*: differences and overlap. *Biol. Bull.* **163**, 144–153.

Gleeson, R. A. (1982). Morphological and behavioral identification of the sensory structures mediating pheromone reception reception in the blue crab, *Callinectes sapidus*. *Biol. Bull.* **163**, 162–171.

Gleeson, R. A., Carr, W. E. S. and Trapido-Rosenthal, H. G. (1993). Morphological characteristics facilitating stimulus access and removal in the olfactory organ of the spiny lobster, *Panulirus argus*: insight from the design. *Chem. Senses* **18**, 67–75.

Gleeson, R. A., McDowell, L. M. and Aldrich, H. C. (1996). Structure of the aesthetasc (olfactory) sensilla of the blue crab, *Callinectes sapidus*: transformations as a function of salinity. *Cell Tissue Res.* **284**, 279–288.

Gomez, G., Voigt, R. and Atema, J. (1999). Temporal resolution in olfaction. III. Flicker fusion and concentration-dependent synchronization with stimulus pulse trains of antennular chemoreceptor cells in the American lobster. *J. Comp. Physiol.* A **185**, 427–436.

Grünert, U. and Ache, B. W. (1988). Ultrastructure of the aesthetasc (olfactory) sensilla of the spiny lobster, *Panulirus argus*. *Cell Tissue Res.* **251**, 95–103.

Hallberg, E., Johansson, K. U. I. and Elofsson, R. (1992). The aesthetasc concept: structural variations of putative olfactory receptor cell complexes in Crustacea. *Microsc. Res. Tech.* **22**, 325–335.

Hallberg, E., Johansson, K. U. I. and Wallén, R. (1997). Olfactory sensilla in crustaceans: morphology, sexual dimorphism and distribution patterns. *Int. J. Insect Morph. Embryol.* **26**, 173–180.

Hansen, B. and Tiselius, P. (1992). Flow through feeding structures of suspension feeding zooplankton: A physical model approach. *J. Plankton Res.* **14**, 821–834.

Heimann, P. (1984). Fine structure and molting of the aesthetasc sense organs on the antennules of the isopod, *Asellus aquaticus* (Crustacea). *Cell Tissue Res.* **235**, 117–128.

Hood, D. C. and Grover, B. G. (1974). Temporal summation of light by a vertebrate visual receptor. *Science* **184**, 1003–1005.

Kaissling, K.-E. (1998a). Flux detectors *versus* concentration detectors: two types of chemoreceptors. *Chem. Senses* **23**, 99–111.

Kaissling, K.-E. (1998b). Pheromone decativation catalyzed by receptor molecules: a quantitative kinetic model. *Chem. Senses* **23**, 383–395.

Koehl, M. A. R. (1993). Hairy little legs: feeding, smelling and swimming at low Reynolds numbers. *Contemp. Math.* **141**, 33–64.

Koehl, M. A. R. (1995). Fluid flow through hair-bearing appendages: feeding, smelling and swimming at low and intermediate Reynolds numbers. In *Biological Fluid Dynamics* (ed. C. P. Ellington and T. J. Pedley). *Soc. Exp. Biol. Symp.* **49**, 157–182. Cambridge: Company of Biologists Limited.

Koehl, M. A. R. (1996a). Small-scale fluid dynamics of olfactory antennae. *Mar. Fresh. Behav. Physiol.* **27**, 127–141.

Koehl, M. A. R. (1996b). When does morphology matter? *Annu. Rev. Ecol. Syst.* **27**, 501–542.

Lanchester, W. F. (1903). Stomatopoda, with an account of the varieties of *Gonodactylus chiragra*. Marine Crustaceans, VIII. In The fauna of the Maldive and Laccadive Archipelagoes: being an account of the work carried out and of the collections made by an expedition during the years 1899 and 1900. **1**, 444–459.

Louden, C., Best, B. and Koehl, M. A. R. (1994). When does motion relative to neighboring surfaces alter the flow through arrays of hairs? *J. Exp. Biol.* **193**, 233–254.

Mead, K., Koehl, M. A. R. and O'Donnell, M. J. (1999). Stomatopod sniffing: the scaling of chemosensory sensilla and flicking behavior with body size. *J. Exp. Mar. Biol. Ecol.* **241**, 235–261.

Rospars, J.-P., Křivan, V. and Lánsky, P. (2000). Perireceptor and receptor events in olfaction. Comparison of concentration and flux detectors: a modeling study. *Chem. Senses* **25**, 293–311.

Rubenstein, D. I. and Koehl, M. A. R. (1977). The mechanisms of filter feeding: some theoretical considerations. *Am. Nat.* **111**, 981–994.

Sandeman, R., Clarke, D., Sandeman, D. and Manly, M. (1998). Growth-related and antennular amputation-induced changes in the olfactory centers of crayfish brain. *J. Neurosci.* **18**, 6195–6206.

Schmitt, B. C. and Ache, B. W. (1979). Olfaction: responses of a decapod crustacean are enhanced by flicking. *Science* **205**, 204–206.

Shimeta, J. (1993). Diffusional encounter of submicrometer particles and small cells by suspension feeders. *Limnol. Oceanogr.* **38**, 456–465.

Shimeta, J. and Jumars, P. (1991). Physical mechanisms and rates of particle capture by suspension feeders. *Oceanogr. Mar. Biol. Annu. Rev.* **29b**, 191–257.

Snow, P. J. (1973). Ultrastructure of the aesthetasc hairs of the littoral decapod, *Paragrapsus gaimardii*. *Z. Zellforsch.* **138**, 489–502.

Sokal, R. R. and Rohlf, F. J. (1995). *Biometry*, third edition. New York: W. H. Freeman & Company. 887pp.

Vogel, S. (1994). *Life in Moving Fluids*, second edition. Princeton, NJ: Princeton University Press. 467pp.

Zimmer-Faust, R. K. (1989). The relationship between chemoreception and foraging behavior in crustaceans. *Limnol. Oceanogr.* **34**, 1364–1374.